# Fracture size effect in ultrananocrystalline diamond: Applicability of Weibull theory

B. Peng, C. Li, N. Moldovan, and H.D. Espinosa[a)]
*Department of Mechanical Engineering, Northwestern University, Evanston, Illinois 60208-3111*
X. Xiao, O. Auciello,[b)] and J.A. Carlisle
*Materials Science Divisions, Argonne National Laboratory, Argonne, Illinois 60439*

(Received 18 March 2006; accepted 29 June 2006)

An analysis of size effects and doping on the strength of ultrananocrystalline diamond (UNCD) thin films is presented. The doping was achieved by the addition of nitrogen gas to the $Ar/CH_4$ microwave plasma. The strength data, obtained by means of the membrane deflection experiment (MDE) were interpreted using Weibull statistics. The validity and predictive capability of the theory were examined in conjunction with detailed fractographic and transmission electron microscopy microstructural analysis. The Weibull parameters were estimated nonlinear regression based on 480 tests when the specimen volume varied from 500 to 16,000 $\mu m^3$. Both undoped and doped UNCD films exhibited a decrease in strength with an increase in specimen size. A significant drop in strength was measured when the films were doped with nitrogen. Such a drop was almost independent of the percentage of doping. The results also showed that one can predict the fracture strength of a component possessing any arbitrary volume to within ±3%. Moreover, the failure mode of UNCD was found to be volume controlled. We also report changes in Young's modulus as a function of doping for *n*-doped UNCD thin films.

## I. INTRODUCTION

Failure of brittle materials is caused by the unstable propagation of microcracks that initiate at surface or volume defects. Typically, such defects exhibit a random distribution of size, orientation, and location. At the millimeter or larger size scale, where microstructure details are averaged, material strength does not strongly depend upon the size and shape of the test specimen. Other characteristics of the system such as the size of the process zone ahead of a crack tip become dominant. However, at the micron and sub-micron scale, where the number of defects can be greatly reduced by decreasing the size of the interrogated volume or surface, fracture strength is strongly size dependent. This size effect can be explained by the statistical theory first proposed by Weibull.[1,2] This theory describes strength variability in brittle materials by means of well-defined statistical parameters. Hence, knowledge of these material parameters, i.e., Weibull modulus and characteristic strength, is the first step in developing predictive capabilities in applications of interest, for instance, microelectromechanical systems (MEMS).[3,4]

The existence of size effect in brittle MEMS materials has been reported by LaVan et al.,[5,6] Sharpe et al.,[3,4,7] Espinosa et al.,[8,9] Bagdahn et al.,[3] Chasiotis et al.,[10,11] and Chen et al.[12] LaVan et al. arranged a cross-comparison of the strength of Sandia polysilicon as identified by various laboratories.[5,6] All the samples were fabricated with a thickness of 2.5 μm while the sample lengths ranged from 15 to 1000 μm long. Five laboratories, LaVan et al.,[5] Tsuchiya et al.,[13] Sharpe et al.,[4] Chasiotis and Knauss,[10,11] and Read et al.,[14] tested the same samples with various methodologies. Although the results varied from group to group they all found a strong size effect in the strength of the polysilicon specimens. Weibull analysis predicted a general tendency for strength to increase with decreasing specimen size.

Sharpe et al.[4] created a novel specimen design and loading mechanism that permitted testing of polysilicon specimens of various thickness, widths, and lengths. The specimens were 1.5, 2.0, and 3.5 μm thick, 6, 20, and 600 μm wide, and 250, 1000, and 4000 μm long. The measured Young's modulus had a value of 158 ± 10 GPa

[a)]Address all correspondence to this author.
e-mail: espinosa@northwestern.edu
[b)]This author was an editor of this journal during the review and decision stage. For the *JMR* policy on review and publication of articles authored by editors, please refer to http://www.mrs.org/jmr_policy.
DOI: 10.1557/JMR.2007.0137

  

with no evidence of substantial specimen size effects. However, the strength exhibited an increase from 1.2 to 1.6 GPa as the specimen size was decreased.[4] In a later paper by Bagdahn et al.,[3] Weibull analysis was used to identify the strength of straight specimens and specimens containing holes or notches leading to stress concentrations. These authors unequivocally demonstrated that Weibull statistics are capable of predicting the strengths of MEMS components. A design methodology was also proposed. In addition, Weibull analysis combined with scanning electron microscopy (SEM) observations showed that strength scales with sidewall area rather than with total surface area or volume.

Chasiotis and Knauss[10,11] performed microtensile tests on elliptically perforated polysilicon specimens. The measured failure strength at the root of a notch increased with decreasing size of the stressed domain. When the notch radius was made as small as 1 μm, the failure stress increased on average by a factor of two relative to the tension values derived from unnotched specimens. They also observed that failure initiation was controlled by the sidewall area of the specimens due to micromachining-induced roughness.

Chen et al.[12] tested mesoscale biaxial flexure and radius hub flexure single-crystal silicon specimens with different surface conditions. The Weibull characteristic strengths of planar biaxial flexure specimens were found to lie in the range of 1.2 to 4.6 GPa. These authors assumed that surface defects instead of bulk defects play a dominant role in determining the strength because of the strong influence of surface finish.

Espinosa et al.[8,9] found similar results in the investigation of ultra-nanocrystalline diamond (UNCD). The strength of 1-μm-thick UNCD thin films decreased from 4.13 to 1.74 GPa when surface roughness increased from 20 to 107 nm [root-mean-square (rms)]. However, the limited number of tested specimens possessing the same surface finish but different volumes prompted these researchers to further examine the validity of Weibull theory in the prediction of UNCD strength.

In this paper, we examine the applicability of the Weibull statistics in the prediction of strength of doped and undoped UNCD thin films. A particular emphasis is placed in assessing the role of volume versus surface in the prediction of the material strength. The article begins with a description of the investigated materials and a short description of the testing methodology followed by the reporting of experimental results including fractographic and transmission electron microscopy (TEM) observations. A statistical analysis of the reported data based on the maximum likelihood estimation is used to identify Weibull parameters. Discussion of results and their implication in the design of MEMS based on UNCD completes the article.

## II. MATERIAL

UNCD, deposited by microwave-plasma-enhanced chemical vapor deposition (MPCVD) with a unique Ar-rich growth chemistry, is distinctive because of its nanostructure.[15] UNCD consists of 3–5 nm $sp^3$-bonded diamond grains separated by narrow grain boundaries that consist of a mixture of $sp^3$ and $sp^2$ bonding.[16] Notably, UNCD has outstanding mechanical properties (~97 GPa hardness, 967 GPa Young's modulus and 4.13 GPa failure strength[9,17]), unique tribological properties (coefficient of friction of the order of ~0.02–0.03[18,19]), and field-induced electron emission (threshold voltage 2–3 V/μm[20]). Electrical conductivity measurements of the nitrogen-doped UNCD films showed that the conductivity increases dramatically (up to 143 $\Omega^{-1}cm^{-1}$) with increasing nitrogen content.[21,22] MEMS/nanoelectromechanical systems (NEMS) applications under investigation include radio frequency (rf) MEMS resonators, bio-MEMS for chemically specific sending,[17,23] nanolithographic techniques, and atomic force microscopy (AFM) potentiometry techniques.[24]

UNCD films (~1 μm thick) were grown on Si substrates. Before deposition, all cleaned Si substrates were ultrasonically seeded by immersing the wafers in a suspension of nano-diamond powders (~5 nm in diameter) in methanol for 30 min, then rinsed with methanol and distilled water sequentially. Undoped UNCD films were deposited in 99% Ar and 1% $CH_4$ mixture at 200 mbars and a total flow rate of 50 sccm. The nitrogen-doped UNCD films were deposited at a pressure of 150 mbar. The $CH_4$ flow rate was fixed at 1sccm, but the nitrogen flow rate varied from 5 to 20 sccm, and the Ar flux decreased correspondingly to maintain the same total flow rate of 100 sccm. The microwave power was 1.2 kW, and the substrate temperature was 800 °C during deposition of both types of films. In this paper, 5% doped UNCD means that during film deposition the percentage of the nitrogen gas is 5% in the total gas flow, and likewise for 10% and 20% doped UNCD. A detailed TEM study of the nanostructure of nitrogen-doped UNCD[22] reveals that nitrogen is being incorporated preferentially at the grain boundaries. High-resolution TEM and nanoprobe-based electron energy-loss spectroscopy indicate that both the grain size and grain-boundary width increase with the increase in nitrogen concentration. The average size of the grains gradually increases from about 4 to 16 nm, as the nitrogen content in the plasma is changed from 0% to 20%. The grain-boundary width increases as well, from about 0.5 to 2.2 nm.[21,22]

To investigate the effect of growth parameters and seeding on material microstructure and surface roughness, freestanding UNCD films were obtained by etching away the substrates. The surface roughness of both undoped and doped UNCD films was identified by AFM.

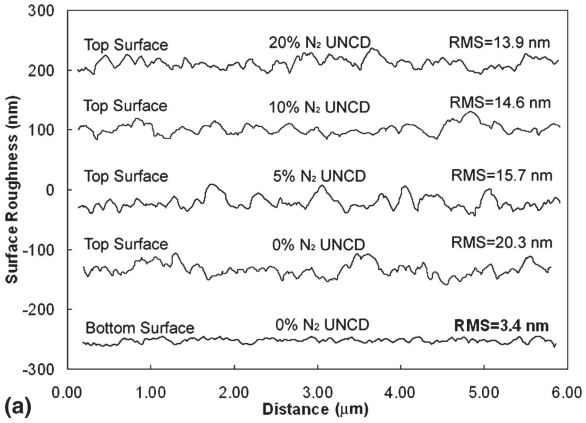


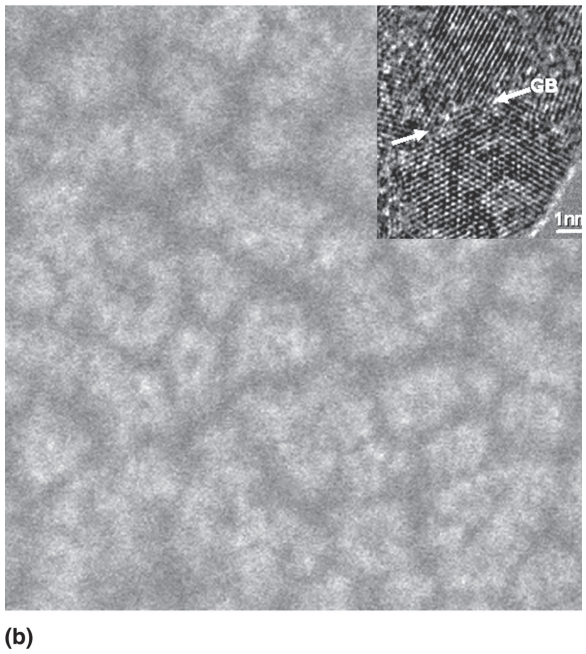


FIG. 1. (a) Surface roughness of UNCD films synthesized with 0%, 5%, 10%, and 20% $N_2$ added to the plasma. Underside roughness is independent of $N_2$ content. (b) SEM micrograph of the underside after etching away; the upper-right window is the TEM cross-section view of the grain structures.

Figure 1(a) shows the surface roughness of the as-deposited UNCD topside and as-etched underside (surface from where film growth starts). Substantial differences in the morphology of these surfaces are observed. The topside is characterized by a rms roughness of 20.3 nm, while the underside is much smoother with a rms of only 3.4 nm. These measurements are consistent with the findings reported by Sumant et al.[18] The study also shows that the topside roughness decreases gradually from 20.3 nm (rms) to 13.9 nm (rms) when the $N_2$ content in the plasma increases from 0% to 20%, while the underside roughness is independent of the $N_2$ content [Fig. 1(a)]. A SEM image of the underside [Fig. 1(b)] reveals small regions, 100–300 nm across, separated by narrow crevices. Sumant et al. referred to these morphological features as "colonies."[18] Each colony appears to have grown outward from a single nucleation site (the seed). These colonies eventually meet and merge on their sides as they grow, thus pinching off the regions now appearing as crevices when imaged from the underside. The topography resembles a two-dimensional analog of grain growth in crystals; however, we highlight that the colonies are not single grains, but grain clusters. Once these colonies coalesce, the remaining UNCD film grows continuously, as revealed by cross-sectional TEM [Fig. 1(b), upper-right window].

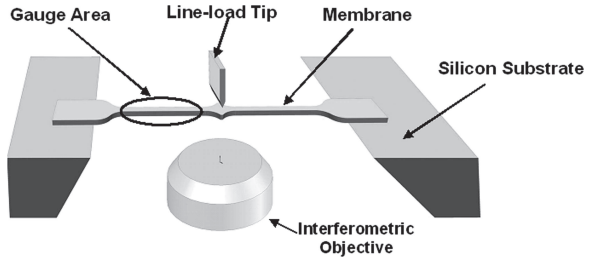


FIG. 2. Schematic illustration showing the membrane deflection experiment setup.

## III. EXPERIMENTAL APPROACH

The nanoindenter load and displacement measurement capabilities were used to perform tensile testing of free-standing UNCD thin films by means of a loading configuration and specimen design in which membrane stressing is achieved. The test is called the membrane deflection experiment (MDE) and consists of transversely loading a membrane that is fixed at both ends and spans a micromachined window (Fig. 2). The membrane has a double dog-bone shape such that bending effects at the ends and where the load is applied do not control failure.[25] Undoped and doped (5%, 10% and 20%) UNCD films were deposited on silicon substrates. Thicknesses were accurately controlled during the deposition process and then measured. Subsequently, the films were patterned using an aluminum masking layer, and the structures were released by potassium hydroxide (KOH) etching from the back side. The details of the specimen microfabrication are reported in Refs. 8 and 9. A calibration plot and more experimental details can be found in Ref. 25, along with the formulas used to compute stress and strain.

In the present study, peak forces were on the order of 15 mN for the 20-μm-wide specimens. The force is estimated to have a relative uncertainty of ±0.6%. The UNCD film thickness was measured by AFM with an uncertainty of ±0.02 μm, and the width was measured by SEM with an uncertainty of ±0.1 μm. The resulting uncertainty in the cross-section area calculation is about ±2.5%. The relative uncertainty of the fracture stress is therefore estimated to be about ±3%.

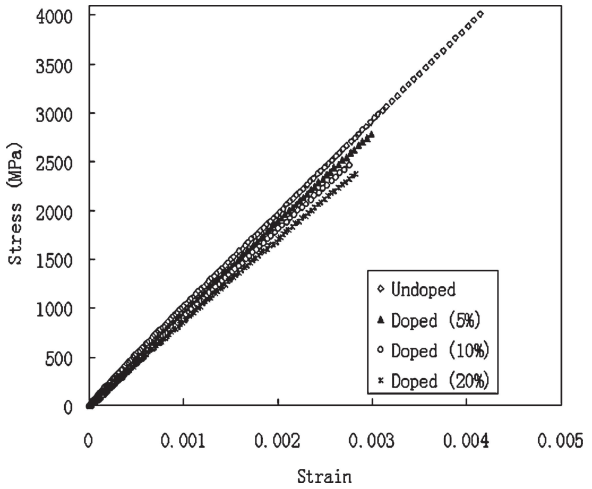


FIG. 3. Strain–stress curves of typical undoped and doped specimens. The maximum stress in each curve represents the characteristic strength $\sigma_0$ of the various materials.

A critical aspect in assessing the applicability of the Weibull theory is the examination of specimens with gauge dimensions spanning a range of volumes and surface areas. For both undoped and doped (5%, 10%, and 20%) UNCD films, specimens with gauge dimensions A (width = 40 μm, length = 400 μm, thickness = 1.0 μm), B (width = 20 μm, length = 200 μm, thickness = 1.0 μm), C (width = 20 μm, length = 200 μm, thickness = 0.5 μm), and D (width = 5 μm, length = 100 μm, thickness = 1.0 μm) were tested to examine the effect of size on strength. Note that gauge volume was varied from 500 to 16,000 $\mu m^3$ while the total surface area was varied from 1,200 to 32,800 $\mu m^2$. Thirty tests were performed for each type of sample exhibiting the same size. Thus, a total of 480 tests were performed.

## IV. EXPERIMENTAL RESULTS

### A. Stress–strain curves

Typical stress–strain curves for undoped and doped (5%, 10% and 20%) UNCD specimens with the same gauge dimensions (width = 20 μm, length = 200 μm, thickness = 1.0 μm) are shown in Fig. 3. The slope of the curve in the linear elastic regime represents the material elastic modulus. The curve for each material is representative of the many samples tested to collect statistical information. The values of the Young's modulus and the characteristic strengths $\sigma_0$ are reported in Table I. The characteristic strength is defined as the stress with a 63% failure probability.

TABLE I. Comparison of Young's moduli and fracture strengths of undoped and doped UNCD.

| Sample | $N_2$ percentage (%) | No. of tests | $E$ (GPa) | $\sigma_0$ (MPa) |
|---|---|---|---|---|
| Undoped | 0 | 30 | 955 ± 25 | 4172 |
| Doped | 5 | 30 | 899 ± 22 | 2713 |
| | 10 | 30 | 867 ± 23 | 2446 |
| | 20 | 30 | 849 ± 19 | 2350 |

Table I and Fig. 3 show that Young's modulus decreases gradually from about 955 GPa to about 849 GPa when the percentage of nitrogen increases from 0% to 20% during the UNCD deposition process. This is likely due to the segregation of nitrogen to the grain boundaries and to the fact that C–N bonds have less stiffness than C–C bonds. Also note that the fracture strength drops abruptly from 4172 MPa to 2713 MPa when $N_2$ increases from 0% to 5%. Then the decline becomes much less pronounced when $N_2$ increases from 5% to 20%.

Using Weibull's "weakest link" theory, we infer that when nitrogen is added into the plasma, defects are produced and/or $N_2$ segregation at the grain boundaries results in a weaker grain/super grain boundary. The presence of nitrogen is enough to produce a major drop in strength, and its increase from 5% to 20% does not seem to modify the strength significantly. The exact mechanism leading to this weakening requires further investigation.

### B. Size effect and Weibull analysis

Traditionally, the size effect has been explained by the Weibull-type weakest-link model.[1,2,26] Its basic hypothesis is that the structure fails as soon as the material strength is exhausted at one point in the structure. Let $P_k$ = failure probability of the $k$th elementary volume ($k = 1, 2, \ldots, N$) and $P_f$ = failure probability of the structure. If the failure of one small elementary volume $V_0$ is assumed to cause the whole structure to fail, then the probability of survival of the structure is the joint probability of survival of all its small elementary volumes, i.e.,

$$1 - P_f = (1 - P_1)(1 - P_2) \cdots (1 - P_N) \quad , \qquad (1)$$

or

$$\ln(1 - P_f) = \sum_{k=1}^{N} \ln(1 - P_k) \approx -\sum_{k=1}^{N} P_k \quad . \qquad (2)$$

The basic idea of Weibull[1] was that the tail of the cumulative distribution of strength must obey a power law, i.e., $P_k = [\sigma(x_k)/\sigma_0]^m$ where $\sigma_0$ and m are material constants called the scale parameter (characteristic strength) and Weibull modulus (shape parameter), and $\sigma(x)$ is the positive part of the maximum principal stress at point $x$. After rearrangements, we obtain

$$P_f = 1 - \exp\left[-\left(\frac{\sigma_N}{\sigma_0}\right)^m\right] \quad , \qquad (3)$$

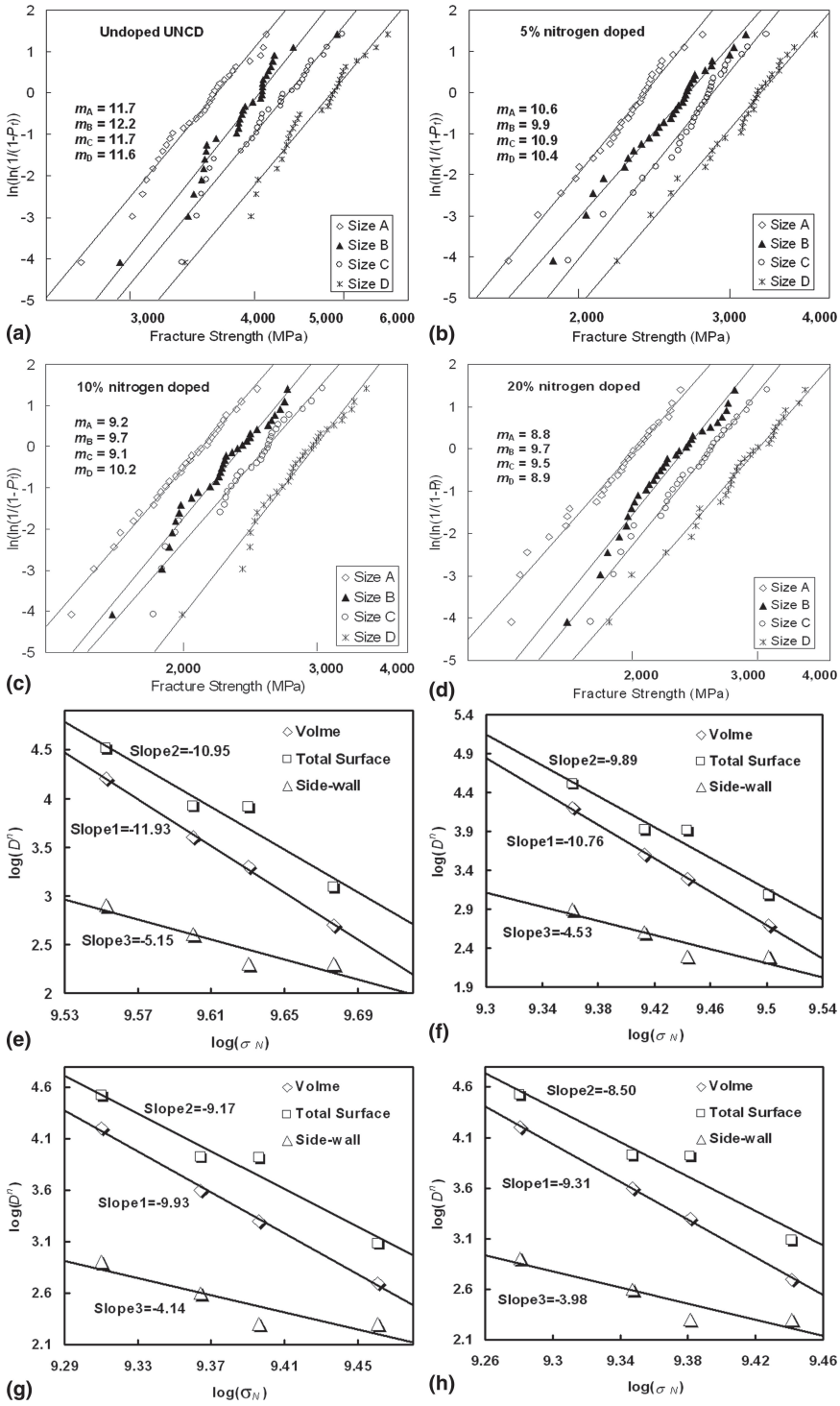


FIG. 4. Weibull plots for various degrees of doping. (a–d) The Weibull modulus and the characteristic strength for each data set are obtained from the straight lines fitted to the data. The linear behavior of the experimental data shows that the Weibull theory is valid. (e–h) Mean nominal strength plotted as a function of the structure volume, total surface area, and side-wall area. The best fit is achieved for the case of volume-distributed defects.

where $\sigma_N$ is the nominal strength. The two Weibull parameters (m and $\sigma_0$) can be obtained from the slope and intercept of a plot [Fig. 4(a)–4(d)] of $\ln\{\ln[1/(1 - P_f)]\}$ versus the measured failure stress $\sigma_N$. Note that this applies to specimens of the same shape and size. To take into account the effect of volumes or areas the probability of failure can be written as

TABLE II. Weibull modulus values, characteristic strengths and the Weibull scale parameters determined from experimental data.

| Sample | $N_2$(%) | Size | No. | m | $\sigma_0$ (MPa) | $\sigma_{0V}$[a] | $\sigma_{0,MLE}$ (MPa) | Error (%) |
|---|---|---|---|---|---|---|---|---|
| Undoped | 0 | A | 30 | 11.7 | 3714 | | 3725 | –0.3 |
| | | B | 30 | 12.2 | 4172 | | 4198 | –0.6 |
| | | C | 30 | 11.7 | 4430 | | 4456 | –0.6 |
| | | D | 30 | 11.6 | 5003 | | 5022 | –0.4 |
| | | MLE Volume | 120 | 11.6 | … | 8581 | | |
| Doped | 5 | A | 30 | 10.6 | 2411 | | 2401 | 0.4 |
| | | B | 30 | 9.9 | 2713 | | 2733 | –0.7 |
| | | C | 30 | 10.9 | 2889 | | 2916 | –0.9 |
| | | D | 30 | 10.3 | 3304 | | 3319 | –0.5 |
| | | MLE Volume | 120 | 10.7 | … | 5933 | | |
| | 10 | A | 30 | 9.2 | 2195 | | 2133 | 2.9 |
| | | B | 30 | 9.7 | 2446 | | 2461 | –0.6 |
| | | C | 30 | 9.1 | 2641 | | 2643 | –0.1 |
| | | D | 30 | 10.2 | 3019 | | 3049 | –1.0 |
| | | MLE Volume | 120 | 9.7 | … | 5786 | | |
| | 20 | A | 30 | 8.8 | 2034 | | 2020 | 0.7 |
| | | B | 30 | 9.7 | 2350 | | 2344 | 0.3 |
| | | C | 30 | 9.5 | 2539 | | 2526 | 0.5 |
| | | D | 30 | 8.9 | 2922 | | 2932 | –0.3 |
| | | MLE Volume | 120 | 9.3 | … | 5719 | | |

*$\sigma_{0V}$ has the unit of MPa × $\mu m^{3/m}$.

$$P_f = 1 - \exp\left[-\int_V \left(\frac{\sigma}{\sigma_{0V}}\right)^m dV\right] \quad ,$$

or

$$P_f = 1 - \exp\left[-\int_A \left(\frac{\sigma}{\sigma_{0A}}\right)^m dA\right] \quad , \tag{4}$$

where $V$ or $A$ is the volume or area of the region stressed in tension, or equivalently,

$$P_f = 1 - \exp\left[-\left(\frac{\sigma_N}{\sigma_{0V}}\right)^m V_e\right] \quad ,$$

or

$$P_f = 1 - \exp\left[-\left(\frac{\sigma_N}{\sigma_{0A}}\right)^m A_e\right] \quad , \tag{5}$$

where $\sigma_{0V}$ and $\sigma_{0A}$ are strengths relative to unit size, and $V_e$ or $A_e$ is the effective volume or area of the samples subjected to uniform stress. The approaches of Eqs. (3) and (5) are related by

$$\sigma_{0V} = V_e^{\frac{1}{m}} \sigma_0 \quad ,$$

or

$$\sigma_{0A} = A_e^{\frac{1}{m}} \sigma_0 \quad . \tag{6}$$

Note that $\sigma_{0V}$ and $\sigma_{0A}$ have the peculiar units of MPa × (memters)$^{3/m}$ or MPa × (memters)$^{2/m}$.

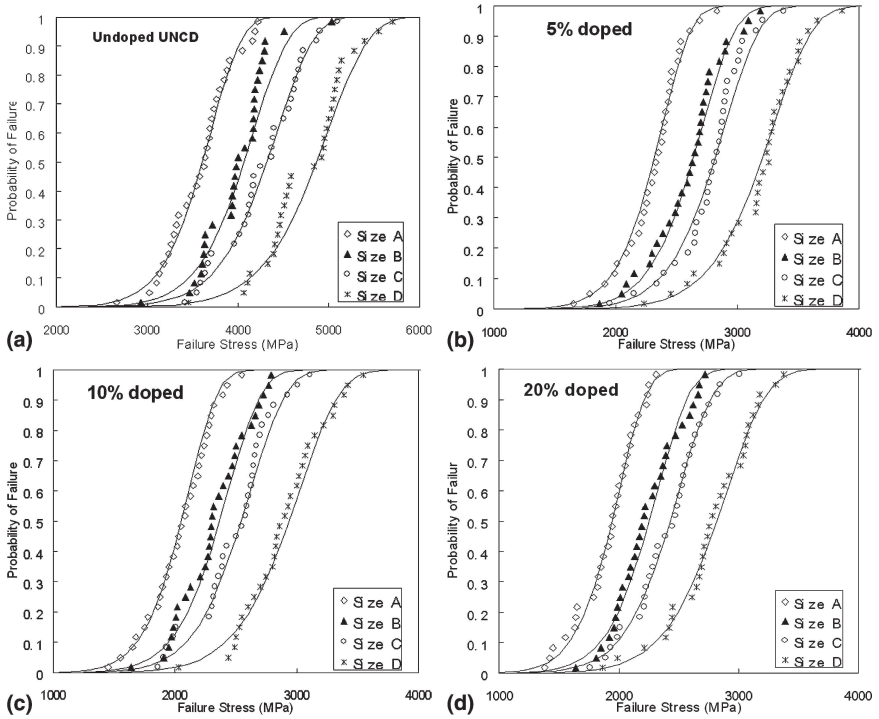


FIG. 5. Experimental results of failure probability versus predicted values. The predicted values are shown as solid lines.

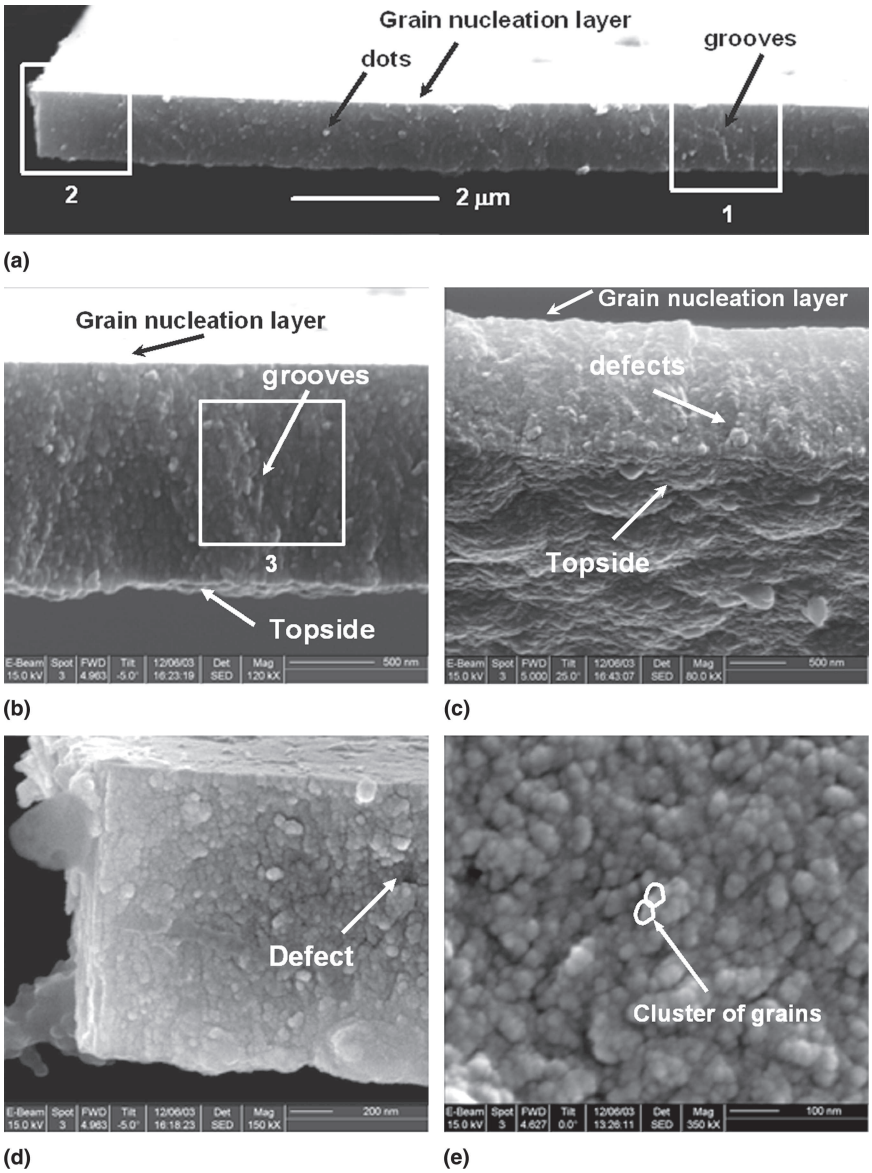


FIG. 6. Fractographic analysis of undoped UNCD specimen. (a) Overall view of the fracture surface with some fracture features. (b) Magnified view of window 1 imaged from the grain nucleation layer. (c) Window 1 imaged from the top surface layer. (d) Window 2 showing the fracture surface near the sample sidewall; no evidence was observed indicating that failure initiated from the side wall. (e) Window 3 showing clusters of grains; note that what appears as grooves at a larger scale becomes a well-defined surface fracture feature consisting of clusters of grains.

Considering now geometrically similar structures of different sizes, the well-known Weibull scaling law for the mean nominal strength can be calculated as a function of size $D$ and geometry parameter $Q$[27];

$$\overline{\sigma}_N(D,Q) = \sigma_0\Gamma\left(1+\frac{1}{m}\right) = C_s(Q)D^{-n/m} \quad , \qquad (7)$$

where

$$C_s(Q) = \Gamma\left(1+\frac{1}{m}\right)\frac{\sigma_0}{Q^{1/m}}V_0^{1/m} \quad . \qquad (8)$$

The power-law size effect in Eq. (7) provides one simple way to identify m. Test data for geometrically similar specimens of different sizes are plotted as $\overline{\sigma}_N$ versus log $D$, and the slope of the regression line of this plot is $-n/m$ ($n$ is the number of spatial dimensions in which the structure is scaled, $n = 1$, 2, or 3.)

The coefficient of variation (CoV) of $\sigma_N$ is calculated as

$$\omega_N = \sqrt{\frac{\Gamma(1+2/m)}{\Gamma^2(1+1/m)} - 1} \quad , \qquad (9)$$

which is independent of structure size as well as geometry.[27]

Figure 4 shows Weibull plots for undoped and doped specimens. For each type of material, four sets of data

were obtained employing sample sizes A–D. In all the performed tests, failure occurred in the gauge area. The modulus m and the characteristic strength $\sigma_0$ were obtained from the straight line fitted to each data set [Figs. 4(a)–4(d)]. These plots suggest that the Weibull theory described above is well-suited for the UNCD material. Moreover, plots of log $D^n$ versus log$\overline{\sigma}_N$ were constructed for various scaling conditions [Figs. 4(e)–4(h)]: volume ($n = 3$), total surface area ($n = 2$), and side-wall area ($n = 2$). Figures 4(e)–4(h) show that for all the tested specimens, the mean nominal strength of the structure is most likely scaled with the volume because the log $D^n$ versus $\overline{\sigma}_N$ plot is linear only when $n = 3$. This result suggests that the failure of UNCD is controlled by a distribution of volume defects. We will reinforce this finding by examination of features in the fracture surfaces and by TEM studies of the tested samples (see fractography and TEM study section). A comparison between the CoV derived from the tested data and the calculated values [from Eq. (9)] was also performed. For undoped UNCD specimens, the coefficient of variations computed from the data are 0.103, 0.097, 0.103, and 0.103 for sizes A–D, respectively; while those calculated from Eq. (7) are 0.103, 0.099, 0.103, and 0.104, which are in excellent agreement. The CoVs for doped specimens were also proved to be independent of the specimen size and geometry.

The Weibull parameters obtained from the tests are summarized in Table II. The scale parameters were determined using maximum likelihood estimation (MLE) based on volume. The MLE method is used to improve the accuracy of the statistical estimation for the Weibull parameters by transferring the four discrete data sets into a single large data set.[28] The last two columns show the predicted characteristic parameters ($\sigma_{0V,\ \mathrm{MLE}}$) and the difference between the predicted values and the measured value. It is shown that the differences are within 2.9%, which means the tests are quite consistent.

Based on the Weibull modulus, the scale parameters and the sample effective volumes, the predicted probability of failure can be calculated from Eq. (5). The predicted values of strengths coincide fairly well with the experimental results (see Fig. 5). Hence, it is reasonable to state that the well-known Weibull theory accurately describes the failure of UNCD in both doped and undoped forms as a function of component size.

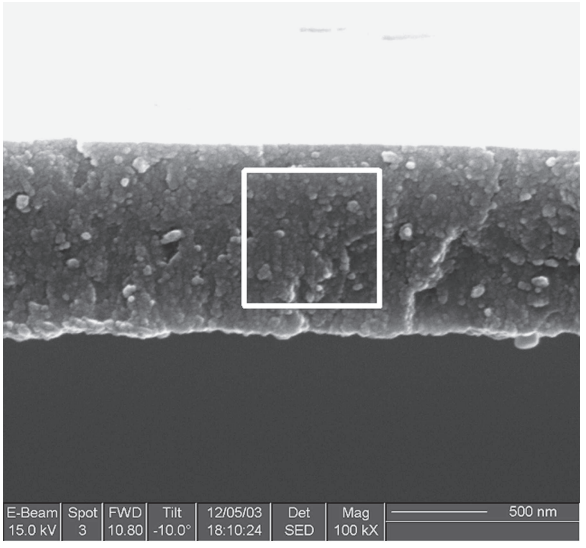


(a)

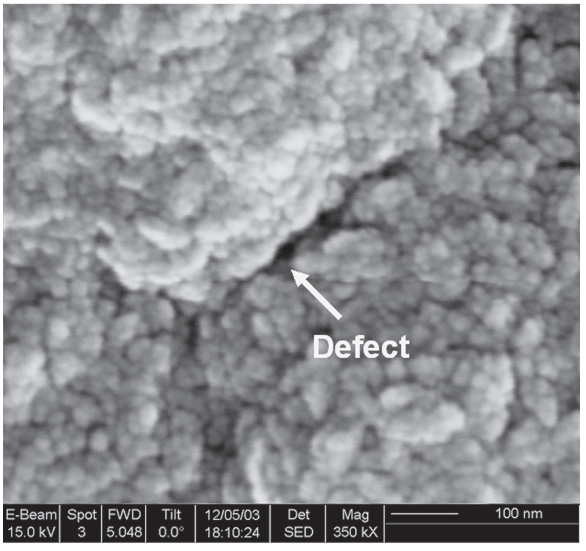


(b)

FIG. 7. (a) Overview of the fracture surface of a 20% $N_2$ UNCD specimen and (b) magnified view of the area within the white rectangle. The arrow in (b) points to a crevasse (possible weak point) in the bulk of the specimen, between 3 larger super-clusters.

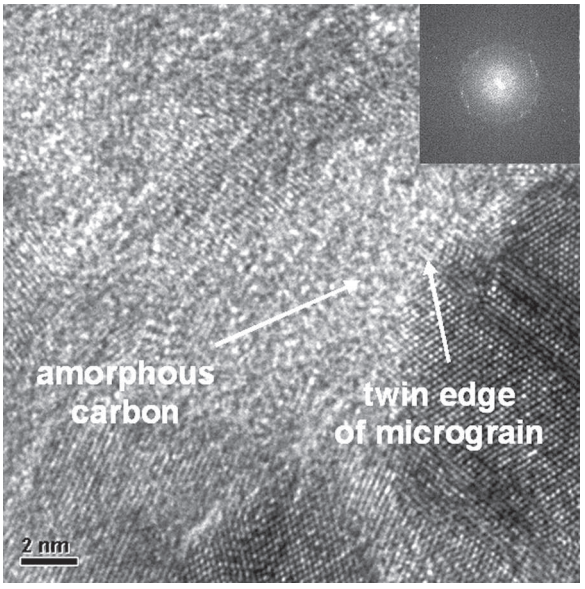


FIG. 8. HRTEM in plan view of a UNCD sample showing amorphous carbon in front of micrograins, one having twins. The inset shows the fast Fourier transform (FFT) of an area within the amorphous region.

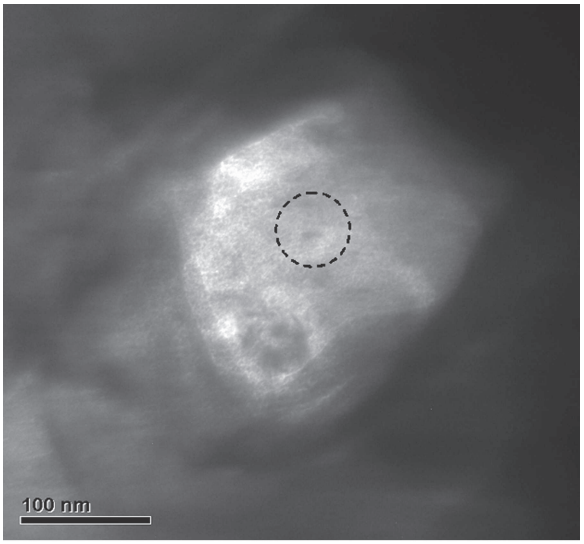


(a)

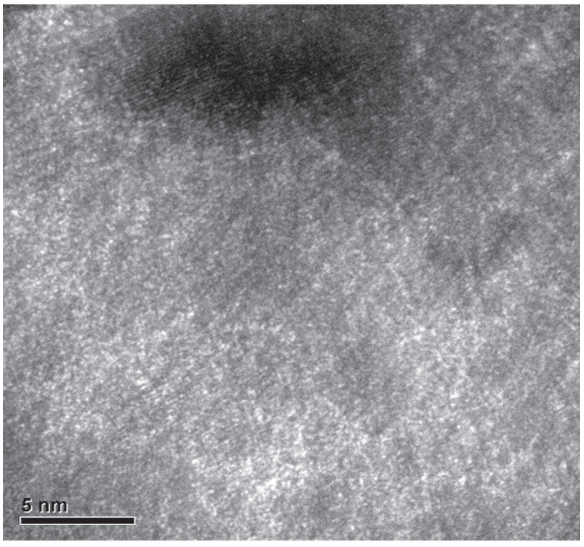


(b)

FIG. 9. (a) Region of UNCD material exhibiting a very large diffraction contrast with its surroundings. (b) Magnified image of the circled area.

## V. FRACTOGRAPHIC AND TEM MICROSTRUCTURAL ANALYSIS

### A. Fractographic analysis

Because the Weibull statistics indicate that failure initiates in the volume of the material, we tried to look in the postmortem fracture areas for typical signs of volume initiated failures and, in the genuine material, to locate inhomogeneities as such eventual sources.

The fracture surfaces were examined with a high-resolution field-emission gun (FEG) SEM. Figure 6 shows a typical fracture surface of an undoped sample at various magnifications. Figure 6(a) is the overall view of the fracture surface. This image is actually upside down with respect to the loading surface (the underside is on the top). Different patterns are observed containing protrusions all over the fracture surface and a series of grooves between them. These features are consistent with intergranular fracture along the cluster boundaries.

In principle, the fracture origin could be on the sidewalls, the top or bottom surfaces, or within the volume. The magnified view of window 1 [Fig. 6(b)] shows that the grain nucleation layer (underside) is much smoother than the surface layer (topside). As mentioned in Sec. II, the grain nucleation layer is composed of many "colonies" with dimensions of 100–300 nm. This nucleation layer is so smooth (rms $=$ 3.4 nm[18]) that it is unlikely to be the origin of the failure. Figure 6(c) shows the same window but from the perspective of the topside. This image clearly reveals that the fracture surface does not follow the valleys of the top and rougher surface. Thorough examination did not reveal any likely fracture initiation from the top surface, while the fracture has a typical granular appearance commonly observed in ceramic fracture surfaces.[3,7,10]

Figure 6(d) shows the edge of the fracture surface (window 2) on the left side wall. Features on this surface are not different from those at the interior. There is no evidence of fracture initiation at the sidewall as was found for poly-silicon.[3,4] The granular appearance of the surface did not permit clear identification of the fracture initiation site, although important microstructural features can be observed. Figure 6(e) (window 3) reveals that the grooves observed in Fig. 6(a) are actually clusters of grains. It is clear that intercluster failure dominates the failure process in the tested UNCD films. Larger crevasses and irregular protrusions suggest the size of the defects is in the range of 20–30 nm [Fig. 6(d)].

The fracture surfaces of doped UNCD are similar to that of undoped UNCD, except that a slightly larger number of defects appear to be present in the fracture surface. Figure 7 reveals what appears to be a small void with a size of approximately 20 nm and the organization of the surrounding clusters (50–100 nm) in superclusters (500–800 nm). This supercluster organization is not typical to the rest of the fracture area, which shows aspects more like Fig. 6(e).

### B. TEM microstructural analysis

The fractographic analysis revealed intercluster inhomogeneities in the volume of the UNCD material as possible fracture initiation sources. However, due to the granularity of the fracture surface, it is not clear if such features were present at those locations before the fracture occurred, or just formed during the brittle fracture process. To investigate the presence of such inhomogeneities in the material microstructure, we performed TEM investigations on several samples prepared by different methods.

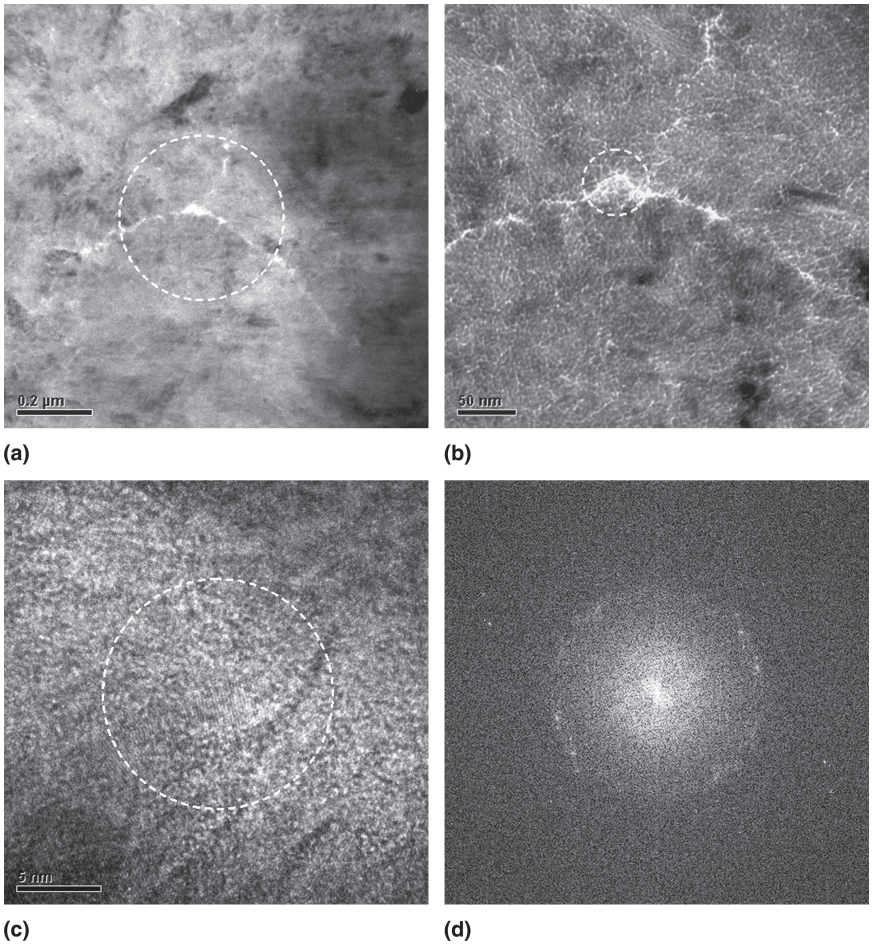


FIG. 10. (a, b) Interclaster pattern observed in undoped UNCD. The circle area in (c) is mostly composed of amorphous carbon and some crystallinity as evidenced by the rings and lattice fringes shown in (d).

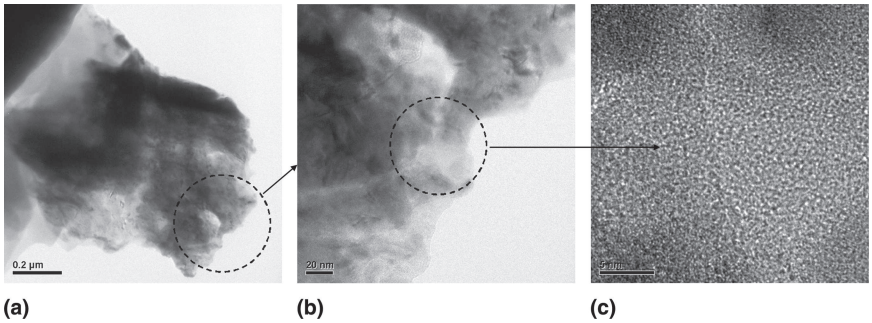


FIG. 11. Sequence of TEM images revealing amorphous carbon at the leading edge of a wedge sample.

Samples were prepared in three modes: (i) plain-view samples were prepared by ion milling and cutting with focused ion beam (FIB) using FEI DB 235 (FEI Company, Hillsboro, OR) equipment; (ii) cross-sectional samples were made by FIB only; and (iii) wedge samples were prepared by growing UNCD on a sharp Si wedge after ultrasonic seeding under the same processing conditions used in the growth of the thin film samples. During ion milling, the energy of the argon ion was 3 keV, and the milling angle was ±6°. While ion milling and FIB machining are standard procedures for TEM samples preparation, they have the disadvantage to potentially change the material by thermal, sputtering, and redeposition processes. Furthermore, long exposures to electron beams during FIB/SEM sample preparation and during TEM imaging can result in the buildup of carbonaceous amorphous species, which may show up in the images but not be part of the original material. The possible

artifacts introduced by ion milling and FIBmachining are avoided in the direct growth of electron transparent thin films of UNCD on Si wedge samples. However, resolution in such samples may be lower due to their higher thickness and its variation across the sample.

TEM observations were performed on a JEOL (Tokyo, Japan) 2010F TEM operated at 200 keV with spherical and chromatic aberration coefficients of 1.0 and 1.4 mm, respectively. In high-resolution TEM (HRTEM) mode, its point and lattice resolution were 0.24 and 0.14 nm, respectively. The TEM observations of undoped UNCD revealed a high microstructural uniformity with grain sizes in the 3–5 nm range, thin inter-grain spacings (2-5 atomic layers), and no visually detectable amorphous regions.[15] However, due to simple statistical fluctuations or small variations in the chemical vapor deposition (CVD) parameters during the growth process, some inhomogeneities are expected to exist. In the following, we emphasize only these anomalies, significant for their potential to act as stress concentrators, without attempting to describe their statistics.

Figure 8 is a TEM image of a plain view through a UNCD sample grown after ultrasonic seeding under the conditions described in Sec. II and no $N_2$ doping. The high-resolution image reveals an inclusion of amorphous carbon among well-defined regular-size diamond grains. The inset shows the ring patterned obtained by fast Fourier transform (FFT). The size of the amorphous region is about 4 × 6 nm, which is of the same order of the grains. Such amorphous regions could be observed in several places of the sample. In one place on the same sample, a small region of size ~100 nm with a very different contrast was also observed (Fig. 9). In one of the samples, a pattern consistent with a boundary between clusters, similar to the crevasses discussed in relation to Fig. 7(b), was observed (Fig. 10). By performing a FFT on a high-magnification image of this boundary, the presence of amorphous carbon was revealed [Figs. 10(c) and 10(d)].

Because all the samples shown in Figs. 8–10 were FIB prepared, a possibility could have been that some of the amorphous regions imaged in the samples were generated during their preparation. However, amorphous regions could also be identified in the wedge grown samples. Figure 11 shows a sequence of TEM images recorded at various magnifications. These images clearly show that the leading edge (growth front) of the undoped UNCD sample present amorphous inclusions. Such inclusions were observed in several locations of the sample. This proves that such material inhomogeneities are distributed in the entire volume of the material and support the volume scaling for the Weibull statistics. While these inhomogeneous regions per se may not result in a major strength reduction, they may cause local deformation modes that can lead to failure initiation. TEM images obtained from 20% $N_2$ doped UNCD samples (Fig. 12) show that the percentage of amorphous carbon in the sample increases significantly. This is consistent with the reduction in $\sigma_0$ reported in Table I.

To summarize, both the fractographic and HRTEM analyses revealed the presence of inhomogeneities in the bulk of the UNCD specimens. The inhomogeneities consist of amorphous regions ranging from 5 to 6 nm between grain clusters and along crevasses between superclusters. We attribute to these inhomogeneities the source of volume-initiated failures.

## VI. DISCUSSION OF RESULTS

The results given in Sec. IV for undoped and doped UNCD specimens demonstrate a clear effect of specimen size on film strength. Likewise, the analysis confirms the validity of Weibull theory in predicting specimen strength when its volume changes by about two orders of magnitude. Because the change in specimen size has limitations, Bagdahn et al.[3] and Chasiotis et al.[11] proposed the usage of specimens with stress concentrations, resulting from holes or notches, to achieve a larger variation in effective volume or surface. Our group recently examined experimentally and theoretically the stress field around notches of different radii to obtain an

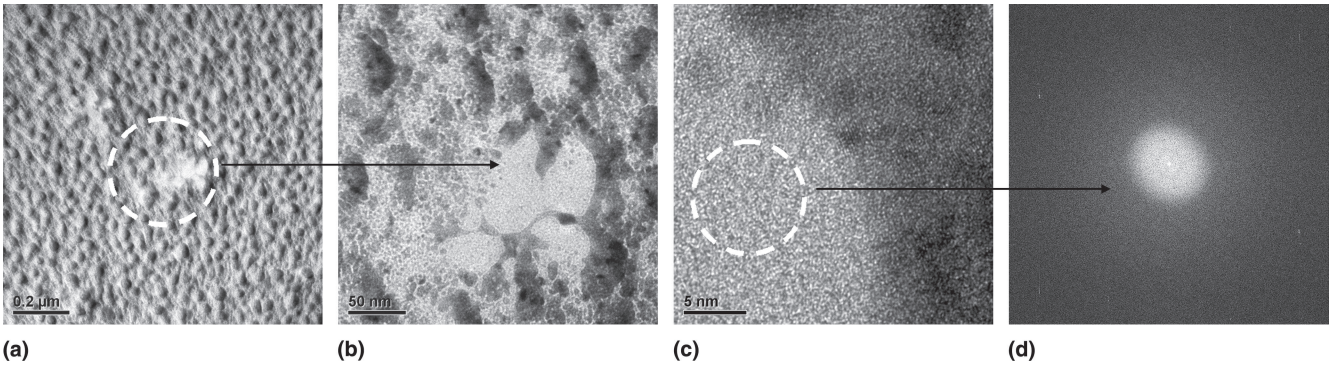


FIG. 12. (a–c) Sequence of images at various magnifications showing microstructural features of UNCD specimen, 20% $N_2$ doped, prepared by FIB. (d) FFT performed on the circled area in (c) revealing amorphous atomic structure.

estimate of defect size in the film and ideal or theoretical strength $\sigma_u$.[29]

The "ideal strength" of brittle materials such as UNCD can be estimated by measuring the fracture toughness $K_{IC}$ and a material characteristic length $d_0$ according to:

$$\sigma_u = \sqrt{\frac{2}{\pi}\frac{{K_{IC}}^2}{d_0}} \quad . \tag{10}$$

The material fracture toughness can be determined by means of the membrane deflection fracture experiment (MDFE) developed by Espinosa and Peng,[30] while the material's characteristic length can be obtained by matching two different experimental results performed on notches with different root radii ρ based on the following equation:

$$K'_{IC} = \sqrt{1 + \frac{\rho}{2d_0}}\, K_{IC} \quad . \tag{11}$$

In this equation, $K'_{IC}$ is the measured fracture toughness with respect to a finite notch radius.[29,30] Accordingly, for the undoped UNCD we estimate $d_0$ by employing $K'_{IC}$ (blunt notch with $\rho \approx 100$nm) of about 6.7 MPa$\sqrt{m}$ and $K_{IC}$ (sharp crack) of about 4.5 MPa$\sqrt{m}$.[30] The corresponding $d_0$ is estimated for undoped UNCD as $d_0^{UNCD} \approx 35$ nm. Furthermore, from Eq. (10) we can estimate the "ideal strength" of the material at the characteristic size of $d_0$ as $\sigma_u^{UNCD} \approx 18$ GPa, which is consistent with the UNCD strength identified in this work based on the Weibull theory. Note that this ideal strength is more than four times greater than the value of $\sigma_0 = 4.17$ GPa reported in Table I.

## VII. CONCLUSIONS

In this work, we investigated the fracture strength of UNCD and the validity of the Weibull statistic analysis. The fracture strength of UNCD thin films is obtained by testing submicron freestanding films by means of the membrane deflection experiment. The Weibull modulus m and the scale parameter $\sigma_0$ are obtained by analyzing the tensile data. The characteristic strengths $\sigma_0$ of undoped and 5%, 10%, 20% $N_2$ doped UNCD films were found to be 4.172, 2.713, 2.446, and 2.350 GPa, respectively. This significant drop in material strength is connected to the increase in defect size within the film as a result of the addition of $N_2$ into the plasma. Both undoped and doped UNCD films exhibit a decrease in strength with increase in homogeneously stressed volume. Data analysis, fractographic observation, and TEM analysis revealed that for ultrasonically seeded films, volume is the "measure" controlling strength size dependence. Our study also shows that Weibull statistics are quite successful in predicting the fracture strength of the tested materials and that this theory can be used with confidence in the design of MEMS devices.

We have also estimated theoretically the ultimate strength of the material, $\sigma_u = 18$ GPa and a characteristic defect size $d_0 = 35$ nm. While more research is needed to assess the accuracy of this prediction, it constitutes a very valuable tool for assessing deposition techniques and process parameters. Likewise, it provides a means for comparing materials to be used in micro and nanodevices.

While in this investigation we have determined that volume is the scaling parameter to be used in the context of Weibull's theory, it is important to keep in mind that process parameters altering surface characteristics may result in a different scaling parameter such as sidewall surface or top surface. In each case, thorough analysis is required to determine the controlling size scale parameter.

## ACKNOWLEDGMENTS

The authors would like to thank Zdenek Bazant for many useful suggestions concerning the interpretation of the experimental results in the context of the applicability of the Weibull statistics. We also acknowledge the contributions of R. Divan and D.C. Mancini in the microfabrication of the UNCD tensile specimens. This work was partially supported by the United States Department of Energy Office of Science under Contract No. N00014-97-1-0550. Work was also supported in part by the National Science Foundation (NSF) Nano Science Interdisciplinary Research Teams (NIRT) under Award No. CMS00304472 and by the NSF under Great Opportunities for Academic Liaison with Industry (GOALI) Award No. CMS-0120866/001.

## REFERENCES

1. W. Weibull: A statistical theory of the strength of materials. *Proc. R. Swedish Inst. Eng. Res.* **151,** 1 (1939).
2. W. Weibull: A statistical distribution function of wide applicability. *J. Appl. Mech.* **18,** 293 (1951).
3. J. Bagdahn, W.N. Sharpe, Jr., and O. Jadaan: Fracture strength of polysilicon at stress concentrations. *J. Microelectromech. Syst.* **12,** 302 (2003).
4. W.N. Sharpe, Jr., K.M. Jackson, J.H. Kevin, and Z. Xie: Effect of specimen size on Young's modulus and fracture strength of polysilicon. *J. Microelectromech. Syst.* **10,** 317 (2001).
5. D.A. LaVan, T. Tsuchiya, G. Coles, W.G. Knauss, I. Chasiotis, and D. Read: Cross comparison of direct strength testing techniques on polysilicon films, in *Mechanical Properties of Structural Films,* edited by C. Muhlstein and S.B. Brown (American Society for Testing and Materials, West Conshohocken, PA, 2001).
6. D.A. LaVan, K. Jackson, S.J. Glass, T.A. Friedmann, J.P. Sullivan, and T. Buchheit: Direct tension and fracture toughness testing using the lateral force capabilities of a nanomechanical test system, in *Mechanical Properties of Structural Films,* edited by C. Muhlstein and S.B. Brown (American Society for Testing and Materials, West Conshohocken, PA, 2001).

7. K.M. Jackson, J. Dunning, C.A. Zorman, M. Mehregany, and W.N. Sharpe, Jr.: Mechanical properties of epitaxial 3C silicon carbide thin films. *J. Microelectromech. Syst.* **14,** 664 (2005).
8. H.D. Espinosa, B. Peng, B.C. Prorok, N. Moldovan, O. Auciello, J.A. Carlisle, D.M. Gruen, and D.C. Mancini: Fracture strength of ultrananocrystalline diamond thin films—Identification of Weibull parameters. *J. Appl. Phys.* **94,** 6076 (2003).
9. H.D. Espinosa, B.C. Prorok, B. Peng, K.H. Kim, N. Moldovan, O. Auciello, J.A. Carlisle, D.M. Gruen, and D.C. Mancini: Mechanical properties of ultrananocrystalline diamond thin films relevant to MEMS/NEMS devices. *Experimental Mechanics* **43,** 256 (2003).
10. I. Chasiotis and W.G. Knauss: The mechanical strength of polysilicon films: Part 1. The influence of fabrication governed surface conditions. *J. Mech. Phys. Solids* **51,** 1553 (2003).
11. I. Chasiotis and W.G. Knauss: The mechanical strength of polysilicon films: Part 2. Size effects associated with elliptical and circular perforations. *J. Mech. Phys. Solids* **51,** 1551 (2003).
12. K.S. Chen, A. Ayon, and S.M. Spearing: Controlling and testing the fracture strength of silicon on the mesoscale. *J. Am. Ceram. Soc.* **83,** 1476 (2000).
13. T. Tsuchiya, J. Sakata, and Y. Taga: Tensile strength and fracture toughness of surface micromachined polycrystalline silicon thin films prepared under various conditions, in *Thin-Films—Stresses and Mechanical Properties VII,* edited by R.C. Cammarata, M. Nastasi, E.P. Busso, and W.C. Oliver (Mater. Res. Soc. Symp. Proc. **505,** Warrendale, PA, 1998), pp. 285–290.
14. D.T. Read, J.D. McColskey, R. Geiss, and Y.W. Cheng: Microtensile testing of thin films in the optical and scanning electron microscopes, in *Characterization and Metrology for ULSI Technology,* edited by D.G. Seiler and A.C. Diebold (AIP Conference Proceedings **683**, 2003), pp. 353–356.
15. D.M. Gruen: Nanocrystalline diamond films. *Ann. Rev. Mater. Sci.* **29,** 211 (1999).
16. D. Zhou, T.G. McCauley, L.C. Qin, A.R. Krauss, and D.M. Gruen: Synthesis of nanocrystalline diamond thin film from an Ar–$CH_4$ microwave plasma. *J. Appl. Phys.* **83,** 540 (1998).
17. O. Auciello, J. Birrell, J.A. Carlisle, J.E. Gerbi, X. Xiao, B. Peng, and H.D. Espinosa: Materials science and fabrication processes for a new MEMS technology based on ultrananocrystalline diamond thin films. *J. Phys. Condens. Matter* **16,** R539 (2004).
18. A.V. Sumant, D.S. Grierson, J.E. Gerbi, J. Birrell, U.D. Lanke, O. Auciello, J.A. Carlisle, and R.W. Carpick: Toward the ultimate tribological interface: surface chemistry and nanotribology of ultrananocrystalline diamond. *Adv. Mater.* **17,** 1039 (2005).
19. A. Erdemir, G.R. Fenske, A.R. Krauss, D.M. Gruen, T. McCauley, and R.T. Csencsits: Tribological properties of nanocrystalline diamond films. *Surf. Coat. Technol.* **120,** 565 (1999).
20. A.R. Krauss, O. Auciello, M.Q. Ding, D.M. Gruen, Y. Huang, V.V. Zhirnov, E.I. Givargizov, A. Breskin, R. Chechen, E. Shefer, V. Konov, S. Pimenov, A. Karabutov, A. Rakhimov, and N. Suetin: Electron field emissions for ultrananocrystalline diamond films. *J. Appl. Phys.* **89,** 2958 (2001).
21. B. Bhattacharyya, O. Auciello, J. Birrell, J.A. Carlisle, L.A. Curtiss, A.N. Goyette, D.M. Gruen, A.R. Krauss, J. Schlueter, A. Suman, and P. Zapol: Synthesis and characterization of highly-conducting nitrogen doped ultrananocrystalline diamond films. *Appl. Phys. Lett.* **79,** 1441 (2001).
22. J. Birrell, J.A. Carlisle, O. Auciello, D.M. Gruen, and J.M. Gibson: Morphology and electronic structure in nitrogen-doped ultrananocrystalline diamond. *Appl. Phys. Lett.* **81,** 2235 (2002).
23. W. Yang, O. Auciello, J.E. Butler, W. Cai, J.A. Carlisle, J.E. Gerbi, D.M. Gruen, T. Knickerbocker, T.L. Lasseter, J.N. Russell, L.M. Smith, and R.J. Hamers: DNA-modified nanocrystalline diamond thin-films as stable, biologically active substrates. *Nat. Mater.* **1,** 253 (2002).
24. K-H. Kim, N. Moldovan, C. Ke, H.D. Espinosa, X. Xiao, J.A. Carlisle, and O. Auciello: Novel ultrananocrystalline diamond probes for high-resolution low-wear nanolithographic techniques. *Small* **1,** 866 (2005).
25. H.D. Espinosa, B.C. Prorok, and M. Fisher: A methodology for determining mechanical properties of freestanding thin films and MEMS materials. *J. Mech. Phys. Solids* **51,** 47 (2003).
26. W. Weibull: The phenomenon of rupture in solids. *Proc. R. Swedish Inst. Eng. Res.* **153,** 1 (1939).
27. Z.P. Bazant, Y. Zhou, D. Novak, and I.M. Daniel: Size effect on flexural strength of fiber-composite laminates. *J. Eng. Mater. Technol.* **126,** 29 (2004).
28. C.A. Johnson and W.T. Tucker: Advanced statistical concepts of fracture in brittle materials. *Eng. Mater. Handbook, Ceram. Glasses* **4,** 709 (1991).
29. N. Pugno, B. Peng, and H.D. Espinosa: Prediction of strength in MEMS components with defects—A novel experimental-theoretical approach. *Int. J. Solid Struct.* **42,** 647 (2005).
30. H.D. Espinosa and B. Peng: A new methodology to investigate fracture toughness of freestanding MEMS and advanced materials in thin film form. *J. Microelectromech. Syst.* **14,** 153 (2005).